Comprehensive Battery Safety Risk Evaluation: Aged Cells versus Fresh Cells Upon Mechanical Abusive Loadings

Yikai Jia, Xiang Gao, Lin Ma,* and Jun Xu*

Despite their wide applications, lithium-ion batteries (LIBs) have been struggling with their safety risks arising from different lifetime stages. Here, the NCMA pouch cell is taken as an example, and the safety of both fresh and aged cells from three milestone stages, that is, internal short circuit (ISC) triggering risk, ISC mode, and the subsequent thermal runaway (TR) consequence is investigated. By combining mechanical abusive testing and physics-based models on commercialized cells with various states-of-health (SOH) and states-of-charge, it is discovered that the ISC triggering delays with the decay of SOH and soft ISC mode will be triggered more frequently, which is mainly due to the mechanical behaviors of the current collectors. The temperature rises and peak temperature during the subsequent TR also become milder for aged cells due to the reduced capacity and deterministic soft ISC process. Results here provide a mechanistic explanation of the safety risk comparison between the fresh and aged cells, offering cornerstone guidance to the evaluation and design of next-generation safer LIBs.

1. Introduction

As one of the most promising energy storage systems, lithium-ion batteries (LIBs) are widely and increasingly applied in various devices and facilities, such as smartphones,[1] laptops,[2] electric vehicles,[2,3] and energy storage power stations.[4] During the

Y. Jia, X. Gao, L. Ma, J. Xu
Department of Mechanical Engineering and Engineering Science
The University of North Carolina at Charlotte
Charlotte, NC 28223, USA
E-mail: l.ma@uncc.edu; jun.xu@uncc.edu
Y. Jia, X. Gao, L. Ma, J. Xu
Battery Complexity
Autonomous Vehicle
and Electrification (BATT CAVE) Research Center
University of North Carolina at Charlotte
Charlotte, NC 28223, USA
J. Xu
School of Data Science
University of North Carolina at Charlotte
Charlotte, NC 28223, USA

long-term service in a few years, those devices or facilities may have internal cycling degradation and inevitably sustain certain types of external abusive loading.[3] Particularly, the most common challenging scenario that we face in real-world engineering applications is the combination of cycling degradation and abusive loading. Thus, the safety risk evaluation of aged cells is equally important as fresh cells.

Quite a few pioneering works have focused on the hazardous consequences of fresh LIBs upon abusive loadings.[5] Safety behaviors of LIBs are usually characterized by experiments. Mechanical,[6] electrical,[7] and thermal abusive loading[8] are three typical types of battery safety tests. Under typical mechanical abusive loading, for example, compression,[9] indentation,[9,10] bending,[9,10b,11] and penetration,[12] the deformation or failure of the constituent material,[9,10b] is the fundamental reason cause the contact between the anode and cathode,[13] defined as the internal short circuit (ISC). Similarly, the ISC can also be triggered by electrical abusive loadings, like over-charging or over-discharging,[14] and thermal abusive loading, such as external heating,[15] or phase change materials.[16] The ISC would produce massive heat and trigger exothermic reactions.[17] A subsequent thermal runaway (TR) may be triggered when the exothermic reactions become violent.[5] As one of the most severe consequences that could cause fatality incidents, the TR is usually accompanied by intense energy released and smoke/fire/explosion.[18] The TR could also trigger the TRs of the neighboring batteries and propagate within the battery pack. The TR propagation can lead to more catastrophic hazards.[8,19]

Compared with fresh cells, aged cells may have some performance degradation caused by, for example, loss of lithium inventory and loss of active material.[20] Those degradation mechanisms also have a non-trivial impact on battery safety behaviors.[20,21] In terms of mechanical behaviors, cycling age reduces Young's modulus and failure stress based on the compression and tensile tests of battery components.[22] Intercalation of particles in the separator pores was found to lead to the reduction in the failure force of the cycle-aged nickel oxide batteries.[23] The mechanism for the mechanical behavior changes of cycled cells under the indentation test based on several characterization experiments is the irreversible swelling of the battery leading to the shift in the displacement in the force–displacement curves.

**ADVANCED
SCIENCE NEWS**

www.advancedsciencenews.com

**ADVANCED
ENERGY
MATERIALS**

www.advenergymat.de

Also, the electrolyte consumption caused the changes in mechanical properties of the separator and active materials, and further led to the higher failure force.[21a] These findings indicate a deteriorated mechanical integrity for aged cells. Regarding thermal behaviors, the changes in the battery TR performance of cycled cells vary with chemistries and operating conditions.[20] Some research work showed that cycled batteries show higher instability (lower triggering temperature and higher self-heating rate),[24] while others observed improved thermal stability due to the capacity loss.[25] One step further, it is reported that TR behavior of a large format LIB is aging path dependent.[20]

Generally, the safety risks of the cells are usually characterized by three aspects, that is, 1) electrochemical integrity (easiness to trigger ISC), 2) ISC behavior (voltage behavior and contact resistance in ISC), and 3) thermal instability (heat generation/temperature increase in TR). Electrochemical integrity is fundamentally induced by the physical contact between the cathode and anode.[26] Thus, physical deformation and failure behaviors of the component materials (especially for the separator[10a]) for LIBs determine the electrochemical integrity. The triggered ISC mode is also determined by the involving pair constituent materials and areas where direct physical contacts occur.[26,27] The early triggering of ISC does not necessarily indicate a violent/major ISC mode since various ISC modes lead to different temperature rising behaviors coupled with the sidereactions.[11] Thermal instability is dependent on the fundamental thermal properties of the materials and highly related to the ISC behaviors.[28] These three aspects together constitute a complete evaluation domain for battery safety risk. However, all the available research efforts focus on a single aspect of the safety risk, which leads to biased conclusions.

Herein, in this paper, we evaluate the safety risk of LIBs by using a representative type of $Li[Ni_{1/3}Co_{0.233}Mn_{1/3z}Al_{0.1}]O_2$/graphite commercialized pouch cells from the starting of ISC triggering, ISC behavior, and the consequence temperature rising behaviors. We leverage the mechanical indentation with a steel ball to trigger highly repeatable and controllable ISC behaviors without introducing extra external energy to the system (i.e., the cell). The peak force, the nominal ISC strain, the average voltage change rate, the average temperature change rate, and the temperature rise are used as critical indicators to quantitatively measure the safety risk. Validated physics-based models assist and complement the experimental characterization to explain the fundamental mechanisms of the safety behaviors.

2. Results

2.1. Sample Preparation and Experimental Designs

Commercially pouch cells with $Li[Ni_{1/2}Co_{7/30}Mn_{1/3}Al_{1/10}]O_2$,[29] graphite anode, and Gen 2 electrolyte (1.2 M $LiPF_6$ dissolved in ethylene carbonate (EC) and ethyl methyl carbonate (EMC) in 3:7 ratio by weight) were selected as the experimental samples (from Hunan Boltpower Storage Technologies Co., Ltd.) (**Figure 1**a). The nominal capacity is 3.2 Ah. The dimensions are $126.5 \times 43.5 \times 6.1$ mm. The mass is 67.8 ± 0.5 g. The sample preparation tests were conducted by the battery tester (Figure 1b). Cells with cycle numbers from 1–300 and state-of-charges (SOCs) from 20% to 100% were prepared (Table S2, Supporting Informa-

tion) (SOC = $Q/Q_{tot} \times 100\%$, where Q is the charging capacity and Q_{tot} is the total capacity measured by constant current–constant voltage (CC–CV) mode charging with $U_{cut} = 4.2V$, $I_{cut} = 1/20C$). Cells were tested using 1C CC–CV charging with a C/20 current limit and 1C CC discharging. The state-of-health (SOH) of the 300-cycle cell decreases by about 2% compared to the fresh cell (Figure 1c) (SOH = $Q_{tot}|_{N=n}/Q_{tot}|_{N=0} \times 100\%$, where N is the cycle number). The voltage change rate of the aged cell is slightly larger than the fresh cell (Figure S4, Supporting Information). The short circuit triggering test was then conducted on the material tester with a safe box and an exhaust fan (Figure 1d). Local mechanical loading with high repeatability[27] was used in the experiment to trigger possible ISC. A 3-mm diameter sphere steel ball was placed on the center of the surface of the cells. During the test, the indenter pressed the ball with a loading speed of 1 mm min^{-1}. The open circuit voltage and surface temperatures (two points: 10/40 mm from the loading point, Figure 1d) were recorded by the multimeter with a frequency of 10 Hz.

2.2. Typical Results

Here, we take a fresh cell with SOC = 100% as a baseline example (**Figure 2**a). Two temperature monitoring points, Point 1 (far end, 40 mm to the loading point) and Point 2 (near-end, 10 mm to the loading point), are set with the measured surface temperatures T_1 and T_2. In terms of the mechanical response, the force increases at first and then drops drastically due to the mechanical failure of the battery components (i.e., casing, anode, separator, and anode).[30] Almost simultaneously, the voltage drops to zero quickly, and both measured temperatures increase drastically. The fracture or deformation of the battery components leads to the contact between anode and cathode,[13] indicating a trigger of the ISC. The cell starts to discharge and the voltage drops. The produced massive heat further triggers the TR reactions.[17] The temperatures keep increasing till all the stored energy is released. T_2 is closer to the ISC area to have a higher increasing rate and larger value than T_1.

First, we employ nominal ISC triggering strain ($\varepsilon_{ISC} = d_{ISC}/h = t_{ISC}v_{load}/h$, where t_{ISC} is ISC time, d_{ISC} is ISC triggering displacement, v_{load} is loading rate, and h is the thickness of the cell), and peak force F_{peak} to indicate the electrochemical integrity of the cell from a mechanical perspective. Previous research indicates that ISC may start from minor ISC (small voltage drop in 0.1–1 mV) and finally develop into an irreversible major ISC.[27] Since this process is short and not obvious in the experiments thus, we define the ISC point as the major ISC in this study (where the voltage dropped significantly without recovering). Second, voltage responses that reflect the ISC evolution process is used to identify the ISC behavior. Finally, the average voltage drop rate ($\Delta U/\Delta t = (U_0 - U_1)/(t_1 - t_{ISC})$, where U_1 is selected as $0.2\%U_{cutoff} \approx 0.01V$ and t_1 is the time when $U = U_1$), average temperature increasing rate (T_2 is selected, $\Delta T/\Delta t = (T_{2,max} - T_{2,0})/(t_{T2} - t_{ISC})$, where $T_{2,max}$ is maximum temperature and t_{T2} is the time when $T_2 = T_{2,max}$), and the highest temperature rise ($\Delta T = T_{2,max} - T_{2,0}$) are defined to evaluate the safety risk of the after ISC risk.

The SOC status of the cell has a significant influence over the mechanical, electrochemical, and thermal behaviors of the
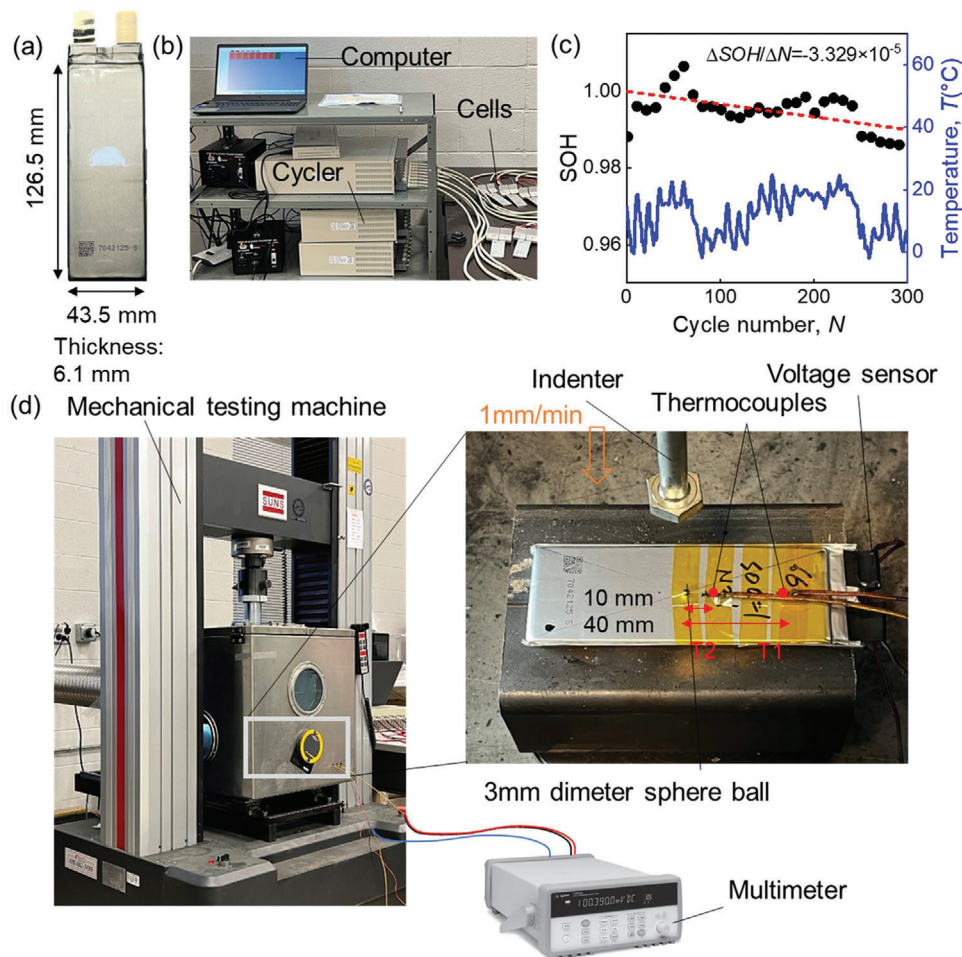
**ADVANCED
SCIENCE NEWS**

www.advancedsciencenews.com

**ADVANCED
ENERGY
MATERIALS**

www.advenergymat.de

Figure 1. Cycling test and short circuit triggering test. a) Dimensions of the sample cell. b) Experimental design of the cycling test. c) Typical SOH–cycle curve of the cells (Note: the temperature obtained from the local meteorological data is for reference). d) Experimental design for the short circuit triggering test.

cell.[31] Here, we confirm that the mechanical performance of the cells has little SOC dependency based on the force–displacement curve (Figure 2b). However, the voltage and temperature responses are highly SOC (initial SOC) dependent (Figure 2c,d). High SOC cells have a quick voltage drop and temperature increase. For the high SOC cells, the cathode at delithiated situation tends to release lattice oxygen. Thus, the total released heat is also larger. TRs were triggered in the cells with SOC ≥ 60%, which can be determined as the SOC-dependent TR onset temperature.[32] Due to a large amount of gas generation, all the cases have expanded significantly (Figure 2e), and all cells in TR have visible burn marks.

3. Discussion

3.1. Short Circuit Triggering Risk

In terms of critical force, the short circuit triggering risk of aged cells has no change compared to fresh cells (**Figure 3**a). F_{peak} has no obvious relationship to both the cycle number N and SOC.

F_{peak} can be expressed by the equation:

$$F_{peak} = \sigma_{ISC} A = \begin{cases} \left(2Rd_{ISC} - d_{ISC}^2\right) \sigma_{ISC}, d_{ISC} < R \\ \pi R^2 \sigma_{ISC}, d_{ISC} \geq R \end{cases} \quad (1)$$

where σ_{ISC} is the nominal stress measured when a short circuit occurs, A is the contact area, and R is the radius of the indenter. Previous results indicate that σ_{ISC} does not change with SOC.[31] The mechanical tests of the battery components, including the anode layer, the cathode layer, and the separator, confirm that the σ_{ISC} of aged cells have no change compared with fresh cells (Figure S1, Supporting Information). Thus, $F_{peak} = \pi R^2 \sigma_{ISC}$ ($d_{ISC} \in [1.6, 1.9]$mm ≥ R = 1.5mm) does not change. Due to the inconsistency of the cells, F_{peak} is distributed in the range of 750–950 N. In terms of critical deformation, the short circuit triggering risk of aged cells is lower than fresh cells (Figure 3b). Nominal ISC strain ϵ_{ISC} is not SOC dependent but positively correlated with N (Figure 3b). ϵ_{ISC} of the aged cells increases by about 14%
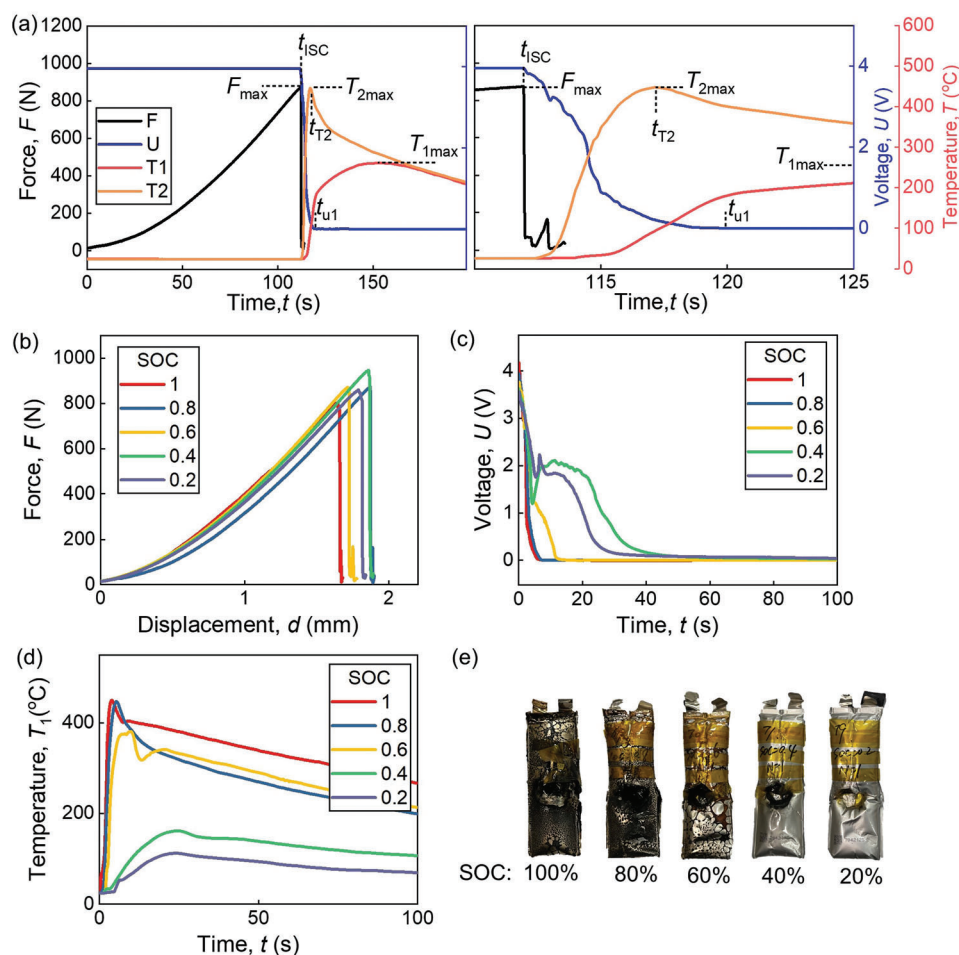
2300368 (3 of 9)

Figure 2. Typical results of the cases with TR triggering. a) Force, voltage, and temperature response and some parameter definitions. b) Force, c) voltage, and d) temperature response of cells with different SOCs. e) Final morphology of the cells.

(Figure 2c). By simple estimation, we may come to

$$\epsilon_{ISC} = \frac{d_{ISC}}{h} = \frac{t_{ISC} v_{load}}{h} \qquad (2)$$

where d_{ISC} is the ISC triggering displacement, h is the thickness of the cell, t_{ISC} is the ISC triggering time, and v_{load} is the loading rate. Compared with the fresh cells, the overall thickness of the cells h increased by about 3% (Figure 3c). Thus, the thickness cannot be a responsible reason since the thickness increase will actually decrease d_{ISC}.

Furthermore, the comparison of nominal stress–nominal strain curves between the fresh and aged cells shows that the material mechanical properties of the anode and separator change little while the cathode has a non-trivial variation (Figure S1a–f, Supporting Information). The mechanical failure strain of the cathode of the aged cell is larger than that in the fresh one (Figure S1c,d, Supporting Information). We also notice that the previous research indicates that Young's modulus E of the cathode aluminum collector may decrease due to some side reactions in cells.[21b] Commonly used hexafluorophosphate (LiPF$_6$) salts are easily decomposed to hy-

drofluoric acid in humid environments, while electrolytes containing commercial bis(trifluoromethane)sulfonamide (LiTFSI) salts tend to corrode the Al current collectors at high potential (> 4 V).[33] To investigate the possible influence caused by Young's modulus, here, we suppose $E_{cycled} = 0.5E_0$ while $E_{fresh} = E_0$, with the assistance of finite element analysis ("Material Tensile Tests and Finite Element Modeling" in Experimental Section). In this case, the cathode collector of the aged cell is softened, and the yield strain ($\epsilon_p = \epsilon - \sigma/E$, where ϵ is the total strain that describes the degree of deformation) is smaller when it is loaded to the same strain (Figure 3d). Thus, the strain at the failure point of the cathode collector will be larger. Further, we exclude the influence brought by coating material properties, and bonding strength between coating and collector via the additional parametric analysis (Table S1, Supporting Information).

Therefore, for the aged cell, the softening of the aluminum foil and a larger failure strain for the cathode together alleviate the possible stress concentrations produced by the crack and edge after the occurrence of fracture. Now it is safe to conclude that ϵ_{ISC} of aged pouch cells increases due to the decrease of E caused by side reactions during cycling.

ADVANCED
SCIENCE NEWS
www.advancedsciencenews.com

ADVANCED
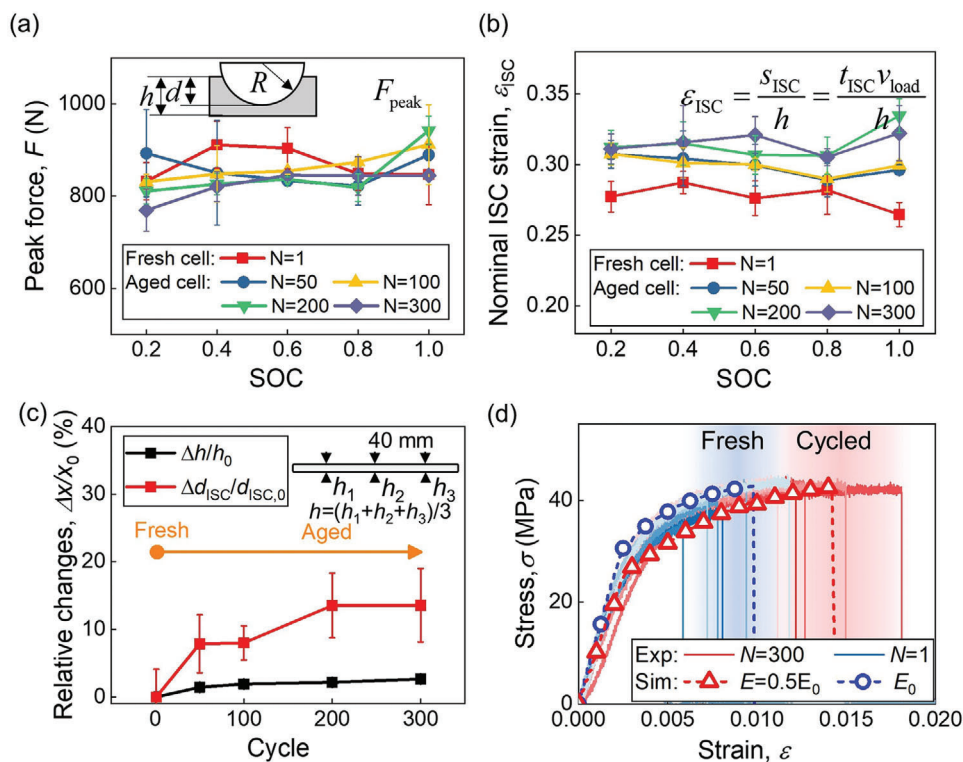**ENERGY**
MATERIALS
www.advenergymat.de

Figure 3. Cycle-aging effects on the mechanical behaviors of the cells. a) Peak force, b) nominal ISC strain, and c) relative thickness. d) Stress–strain curve cathodes at different cycles.

3.2. ISC Modes

Here, we may observe three typical ISC modes: 1) Mode I: TR triggered; 2) Mode II: irrecoverable major ISC and no TR; and 3) Mode III: Voltage recovered with minor ISC (**Figure 4**a). Generally, the cycle-aging effects and the SOC effects are coupled. The ISC mode is highly SOC dependent, as reported and investigated in our previous work.[11,27] Interestingly, the results here indicated that the ISC mode of cells is also highly related to cycled number N. For fresh cells, Modes I, II refer to the cases with large, and small SOC, respectively. However, for aged cells with small and medium SOC, Mode III occurs more frequently (Figure 4a). Different from Mode I/II, the voltage dropped slightly (≈ 0.12 V) and recovered within in few seconds due to the collector melting[11] (Figure 4b). The voltage recovered to a slightly lower value (-0.023 V) than the initial voltage due to the discharging. The voltage then decreases gradually due to the newly exposed contact area with large contact resistance RA produced by the separator melting.[11] Similar to Mode II, the temperature increase in Mode III is also trivial and local. T_2 increases 7.8 °C quickly before the voltage recovery and then increases gradually. T_1 also increases slightly but almost has no increase before the voltage recovery. In terms of the final morphology, there is only permanent deformation left without any massive reaction or flame trace (Figure 4c).

The different ISC modes at high cycle numbers are mainly caused by the different geometric structures caused by the late ISC triggering. The changes are produced by the failure strain/displacement change (ϵ_{ISC} or d_{ISC}) as we discussed above.

To explain the mechanism, we further developed a multiphysics model ("Multiphysics Modeling" in Experimental Section). The multiphysics modeling and related parametric analysis demonstrate that the voltage recovery in this study is related to the deformation of the electrode layers due to the indentation loading (Figure S2, Supporting Information). The voltage recovery occurs when d_{ISC} increases, for example, $d_{ISC} = 1.2 d_{ISC,0}$ (**Figure 5**a and Figure S3, Supporting Information).

When the short circuit is initiated, the short circuit resistance $R_{ISC}(t)$ starts to decrease due to the separator melting (Figure 5b and Figure S3, Supporting Information). The temperature continues to increase. When the local temperature reaches the melting point of the Al collector, the melting of the Al collector also occurs (Figure S3, Supporting Information). When the collector melts, the circuit (cathode collector-indenter-anode collector) is cut off and R_{ISC} increases (Figure 5b). The voltage starts to recover. R_{ISC} is then determined by the new contact between anode coating and cathode coating produced by the separator melting.[11]

Separator melting and Al collector melting occur in both $d_{ISC} = d_{ISC,0}$ and $d_{ISC} = 1.2 d_{ISC,0}$ cases (Figure S3, Supporting Information). The difference is the value of the short circuit resistance $R_{ISC}(t)$ (Figure 5b). At the initial stage, due to the large deformation and small deformed thickness of the layers, R_{ISC} of the aged cell is smaller. When the collector melts, R_{ISC} is then determined by the new contact produced by the separator melting. A thinner electrode layer led to a large transverse resistance. Thus, the aged cell then has a larger R_{ISC}. If R_{ISC} is large enough, the propagation of ISC cannot be maintained (Joule heat power is smaller
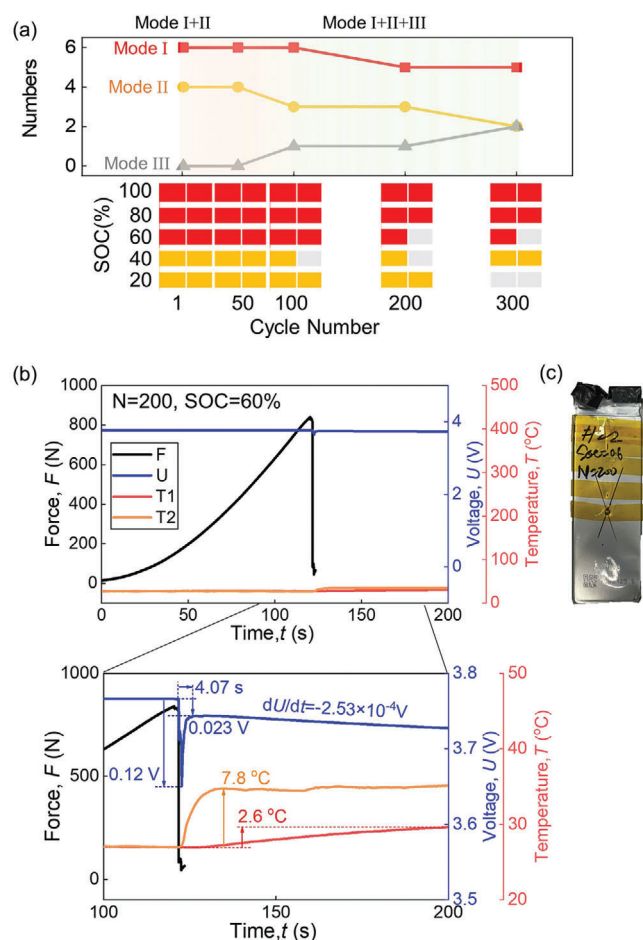
Figure 4. ISC modes under different conditions. a) Case numbers of the three typical behaviors at different cycle numbers. b) Typical behaviors of voltage recovered case.

than the difference between the separator melting heat and dissipation heat).

3.3. Thermal Behaviors after ISC

The voltage change rate $\Delta U/\Delta t$ (absolute value) increases when SOC increases but has no relationship to the cycle number (for Mode III, $U > U_1 = 0.01V$, thus, only Mode I and Mode II are considered here) (**Figure 6**a). However, the temperature rise ΔT_2 and temperature increasing rate $\Delta T_2/\Delta t$ decrease when the cycle number increases, especially for high-SOC cells (Figure 6b,c). The Joule heat, electrochemically generated heat during discharging and exothermic reaction heat are the main heat sources during the ISC and TR.[34] The current pulse tests were conducted at different SOCs and cycle numbers. ±1A currents pulse were selected (Figure S5, Supporting Information) and the internal resistances were estimated by $R_0 = (|\Delta u_1| + |\Delta u_2|)/1A/2$. The pulse current tests show that the internal resistances of the aged cells are close to the fresh cells (Figure 6d), indicating a similar R_{ISC} in both cases. Because $\Delta U/\Delta t$ keep unchanged (Mode I and Mode II), the corresponding electrochemically generated heat and the short circuit Joule heat of aged cells and fresh cells

should be similar. Considering the differences are more obvious in the high SOC cells, therefore, the main reason for the changes in thermal behaviors should be the decrease of the exothermic reaction heat.

The results indicate that the aged NCMA pouch cells exhibit improved thermal stability (temperature rate decreases) and reduced heat generation. These changes can be caused by electrolyte consumption and solid electrolyte interphase (SEI) film thickening.[20,35] Though the onset temperature of self-heating decrease may lead to higher thermal instability, the aged cells in this study are more thermally stable due to the different ISC triggering conditions (i.e., mechanical abusive loading without external constant heat input). The cell is usually uniformly and uninterruptedly heated during the thermal abusive loading condition, thus, the safety hazardous is purely dominated by the TR behavior. The aged cell will be more hazardous if the triggering temperature is lower compared to the fresh cell. However, if the ISC is triggered by a local mechanical abusive loading, the initial ISC is confined within a very localized zone. This localized ISC triggers the TR within a local area, and then the TR propagates to the entire cell. In this case, the cell is not heated uniformly without any external energy input. As such, the heat generation and conduction/radiation process become dominant. The propagation speed is mainly determined by the heat generation rate. Considering that the effects of the low exothermic reaction heat and reaction rate of the aged cell are more obvious, the aged cells are less violent thermally.

4. Conclusion

The safety risk of aged cells is of urgent importance for the further wide application of LIBs while it remains debated. In this work, we proposed a comprehensive methodology to compare the safety risks between the aged and fresh cells. We employed a highly repeatable and controllable mechanical indentation method to trigger the ISC and the possible subsequent TR without the introduction of extra external thermal energy. A type of commercial $Li[Ni_{1/3}Co_{0.233}Mn_{1/3}Al_{0.1}]O_2$/graphite pouch cells was used as the samples. The safety risks were quantitatively evaluated from three aspects: ISC triggering risk, ISC modes, and the subsequent thermal behaviors. The computational results from the physics-based models assisted in explaining the underlying mechanisms. The results indicated that the short circuit triggering risks of the aged pouch cells are lower due to the increased nominal ISC triggering strain. Young's modulus decrease caused by side reactions during cycling leads to the rise of the ISC strain. The ISC modes of the aged pouch cell also become milder. The voltage recovery occurs more frequently in medium SOC cells (SOC from ≈20% to ≈60%) due to the geometrical changes caused by the large ISC triggering strain. In terms of the subsequent thermal behaviors, the aged NCMA pouch cells are also safer due to the decreased temperature change rate and the decreased maximum temperature rise. The possible reasons include the interphasial robustness (e.g., electrolyte consumption and SEI film thickening) and the non-negligible heat generation and conduction during ISC-TR processes.

This work establishes a comprehensive and high-level evaluation understanding and methodology for the safety risk of the cells, clears the mysteries of the safety risk difference between
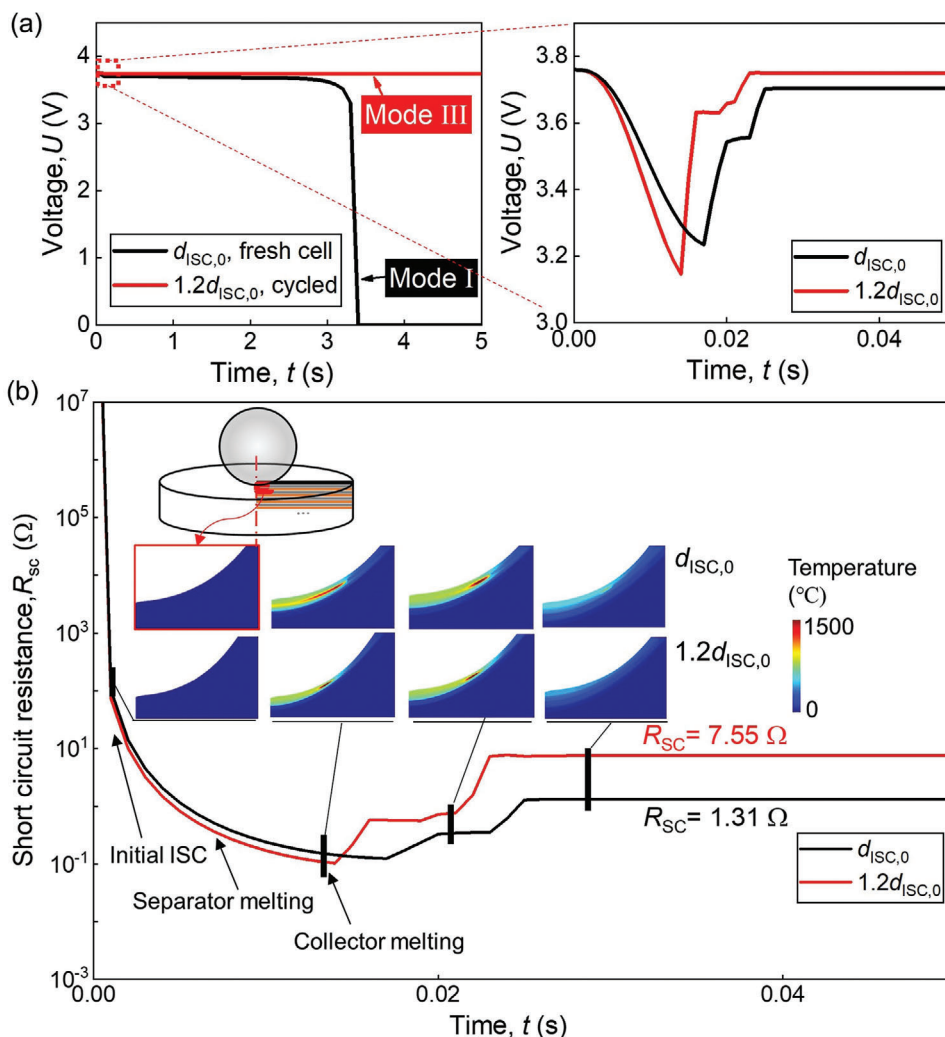
**ADVANCED
SCIENCE NEWS**

www.advancedsciencenews.com

**ADVANCED
ENERGY
MATERIALS**

www.advenergymat.de

Figure 5. ISC evolutional processes. Simulation results of cells with different short circuit triggering displacement: a) voltage curves and b) short circuit resistance curves. (SOC = 60%)

aged and fresh cells, and provides mechanistic guidance for the development, application, and evaluation of the next-generation batteries.

5. Experimental Section

Material Tensile Tests and Finite Element Modeling: The material tensile tests were conducted on the INSTRON E3000 material tester (Figure S6a, Supporting Information). The single layers of the anode, the cathode, and the separator obtained from the sample cells were cut into a rectangular shape with dimensions of 40 mm × 5 mm. The tests were conducted shortly after the sample preparation (within a few minutes). The cathode FE model was developed based on ABAQUS. The same boundary conditions and geometries were used (Figure S6b, Supporting Information). To consider the effect of mechanical property changes in different materials, the coating layer, the bonding layer, and the collector were modeled in detail. The bonding layer was used to simulate the bonding strength between the coating and collector equivalently. The model was used to confirm the effect of the mechanical property changes of the cathode collector. The mechanical properties of other constituent materials

were also discussed to rule out their possibilities (Table S1, Supporting Information).

Multiphysics Modeling: A local-global coupled multiphysics model was developed. The model was developed based on the previous multiphysics models.[11,27] The model contains five sub-models: mechanical model, short circuit model, electrochemical battery model, heat transfer model, and TR model. Those sub-models were developed in different dimensions and were coupled by geometrical and thermal relationships (Figure S7, Supporting Information). The layer structure of the regions around the short circuit point was modeled in detail (Figure S8, Supporting Information). To improve the calculation efficiency, the 2D-axisymmetric model was used. The mechanical model, the short circuit model, and the heat transfer model were used and coupled. The phase changes of the collectors and separators were also considered in the short circuit model. The remaining part of the cell was modeled in a homogenized way. The heat transfer model was used. The 2D local model and 3D global model were coupled by temperature continuity conditions. The electrochemical battery model was modeled in 1D. The TR was described by a group of 0D global ODEs. The electrochemical battery model was validated by charging voltage curves at different C-rates (Figure S9a, Supporting Information). The mechanical model was validated by the indentation test (Figure S9b, Supporting Information). The coupled model was validated
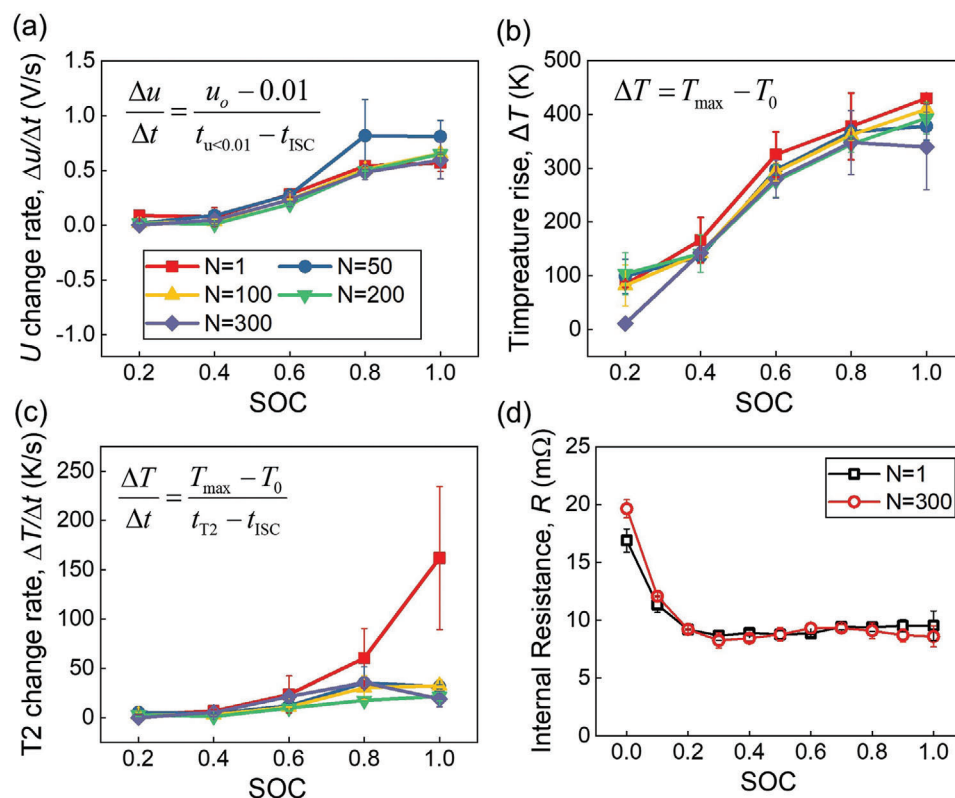
Figure 6. Cycling effects on the thermal behaviors of the cells after ISC. a) Voltage change rate, b) temperature rise, and c) temperature change rate. d) Comparison of internal resistance between 1-cycle cell and 300-cycle cell.

by the voltage and temperature responses of cells with different SOCs after ISC triggering during the indentation tests (Figure S9c,d, Supporting Information).

Supporting Information

Supporting Information is available from the Wiley Online Library or from the author.

Acknowledgements

Conflict of Interest

The authors declare no conflict of interest.

Author Contributions

Y.J.: Methodology, experiment, modeling and writing—original draft; X.G.: Experiment and data analysis; L.M.: Data analysis and writing – review and editing; J.X.: Conceptualization, supervision, methodology, and writing— review and editing.

Data Availability Statement

The data that support the findings of this study are available from the corresponding author upon reasonable request.

Keywords

[1] B. Scrosati, J. Hassoun, Y.-K. Sun, *Energy Environ. Sci.* **2011**, *4*, 3287.
[2] B. Scrosati, J. Garche, *J. Power Sources* **2010**, *195*, 2419.
[3] B. Liu, Y. Jia, C. Yuan, L. Wang, X. Gao, S. Yin, J. Xu, *Energy Storage Mater.* **2020**, *24*, 85.
[4] B. Dunn, H. Kamath, J. M. Tarascon, *Science* **2011**, *334*, 928.
[5] Q. Wang, P. Ping, X. Zhao, G. Chu, J. Sun, C. Chen, *J. Power Sources* **2012**, *208*, 210.
[6] L. Greve, C. Fehrenbach, *J. Power Sources* **2012**, *214*, 377.
[7] P. Bai, J. Li, F. R. Brushett, M. Z. Bazant, *Energy Environ. Sci.* **2016**, *9*, 3221.
[8] D. Ouyang, J. Weng, J. Hu, M. Chen, Q. Huang, J. Wang, *Thermochim. Acta* **2019**, *676*, 205.
[9] J. Xu, B. H. Liu, X. Y. Wang, D. Y. Hu, *Appl. Energy* **2016**, *172*, 180.
[10] a) C. Yuan, L. Wang, S. Yin, J. Xu, *J. Power Sources* **2020**, *467*, 228360; b) L. Wang, S. Yin, J. Xu, *J. Power Sources* **2019**, *413*, 284.
[11] Y. Jia, B. Liu, Z. Hong, S. Yin, D. P. Finegan, J. Xu, *J. Mater. Chem. A* **2020**, *8*, 12472.

[12] D. P. Finegan, B. Tjaden, T. M. M. Heenan, R. Jervis, M. D. Michiel, A. Rack, G. Hinds, D. J. L. Brett, P. R. Shearing, *J. Electrochem. Soc.* **2017**, *164*, A3285.

[13] X. Zhang, E. Sahraei, K. Wang, *Sci. Rep.* **2016**, *6*, 32578.

[14] L. Feng, L. Jiang, J. Liu, Z. Wang, Z. Wei, Q. Wang, *J. Power Sources* **2021**, *507*, 230262.

[15] Z. Huang, T. Shen, K. Jin, J. Sun, Q. Wang, *Energy* **2022**, *239*, 121885.

[16] P. T. Coman, E. C. Darcy, C. T. Veje, R. E. White, *J. Electrochem. Soc.* **2017**, *164*, A587.

[17] X. Feng, Z. Zhang, X. Cui, G. Jin, W. Zheng, H. Liu, *Mater. Lett.* **2018**, *233*, 126.

[18] X. Feng, D. Ren, X. He, M. Ouyang, *Joule* **2020**, *4*, 743.

[19] Y. Jia, M. Uddin, Y. Li, J. Xu, *J. Energy Storage* **2020**, *31*, 101668.

[20] D. Ren, H. Hsu, R. Li, X. Feng, D. Guo, X. Han, L. Lu, X. He, S. Gao, J. Hou, Y. Li, Y. Wang, M. Ouyang, *eTransportation* **2019**, *2*, 100034.

[21] a) G. Kovachev, C. Ellersdorfer, G. Gstrein, I. Hanzu, H. M. R. Wilkening, T. Werling, F. Schauwecker, W. Sinz, *eTransportation* **2020**, *6*, 100087; b) K. Fink, S. Santhanagopalan, J. Hartig, L. Cao, *J. Electrochem. Soc.* **2019**, *166*, A3775.

[22] Z. Wu, L. Cao, J. Hartig, S. Santhanagopalan, *ECS Trans.* **2017**, *77*, 199.

[23] X. Zhang, J. Zhu, E. Sahraei, *RSC Adv.* **2017**, *7*, 56099.

[24] T. Waldmann, J. B. Quinn, K. Richter, M. Kasper, A. Tost, A. Klein, M. Wohlfahrt-Mehrens, *J. Electrochem. Soc.* **2017**, *164*, A3154.

[25] M. Börner, A. Friesen, M. Grützke, Y. P. Stenzel, G. Brunklaus, J. Haetge, S. Nowak, F. M. Schappacher, M. Winter, *J. Power Sources* **2017**, *342*, 382.

[26] S. Santhanagopalan, P. Ramadass, J. Zhang, *J. Power Sources* **2009**, *194*, 550.

[27] B. Liu, Y. Jia, J. Li, S. Yin, C. Yuan, Z. Hu, L. Wang, Y. Li, J. Xu, *J. Mater. Chem. A* **2018**, *6*, 21475.

[28] X. Feng, M. Ouyang, X. Liu, L. Lu, Y. Xia, X. He, *Energy Storage Mater.* **2018**, *10*, 246.

[29] F. Zhou, X. Zhao, Z. Lu, J. Jiang, J. R. Dahn, *Electrochem. Commun.* **2008**, *10*, 1168.

[30] X. Duan, H. Wang, Y. Jia, L. Wang, B. Liu, J. Xu, *Energy Storage Mater.* **2022**, *45*, 667.

[31] J. Xu, B. H. Liu, D. Y. Hu, *Sci. Rep.* **2016**, *6*, 21829.

[32] P. Jindal, J. Bhattacharya, *J. Electrochem. Soc.* **2019**, *166*, A2165.

[33] a) L. Cong, J. Liu, M. Armand, A. Mauger, C. M. Julien, L. Xie, L. Sun, *J. Power Sources* **2018**, *380*, 115; b) H. Zheng, Q. Sun, G. Liu, X. Song, V. S. Battaglia, *J. Power Sources* **2012**, *207*, 134.

[34] G. Liu, W. Lu, *J. Electrochem. Soc.* **2017**, *164*, A1826.

[35] X. Feng, S. Zheng, D. Ren, X. He, L. Wang, H. Cui, X. Liu, C. Jin, F. Zhang, C. Xu, H. Hsu, S. Gao, T. Chen, Y. Li, T. Wang, H. Wang, M. Li, M. Ouyang, *Appl. Energy* **2019**, *246*, 53.